Characterization of Manganese Oxide Octahedral Molecular Sieve (M−OMS-2) Materials with Different Metal Cation Dopants

Xiao Chen,[†] Yan-Fei Shen,[†,‡] Steven L. Suib,*[,†] and C. L. O'Young[§]

Department of Chemistry, Department of Chemical Engineering, Institute of Materials Science, University of Connecticut, Storrs, Connecticut 06269 and Texaco Research Center, Texaco, Inc., P.O. Box 509, Beacon, New York 12508

Received November 1, 2000. Revised Manuscript Received October 5, 2001

Reflux methods were used to prepare different metal cation (M: Cu^{2+}, Zn^{2+}, Ni^{2+}, Co^{2+}, Al^{3+}, or Mg^{2+}) doped manganese oxide octahedral molecular sieve (M−OMS-2) materials with cryptomelane structure. Thorough characterization has been carried out for these M−OMS-2 materials. SEM micrographs of M−OMS-2 materials reveal their typical fibrous morphology. The results of ICP−AES elemental analyses for M−OMS-2 materials shed light on the distribution of doped metal cations in the cryptomelane structure. TGA and XRD studies indicate that the prepared M−OMS-2 materials are more thermally stable in O_2 (up to 600 °C) than in inert (e.g., N_2 or He) atmospheres (up to 500 °C). Phase transformations from cryptomelane to hausmannite or bixbyite were observed when M−OMS-2 materials were heated above these stable temperatures. Comprehensive N_2 sorption analyses confirmed that M−OMS-2 materials are porous materials, which contain micropores and mesopores, with total BET surface areas in the range of 70−110 m^2/g. Basicity studies of synthetic M−OMS-2 materials with TPD of adsorbed CO_2 revealed that all pretreated M−OMS-2 materials have several different basic sites with varied strengths and amounts on their surfaces. TPD studies of NH_3 adsorbed on the pretreated M−OMS-2 materials demonstrate that all M−OMS-2 materials also have similar acidities.

I. Introduction

Microporous molecular sieves have pore dimensions near molecular size. They have been widely used in many chemical processes because of their porous structure, acidity, and ion-exchange abilities. The most common molecular sieve materials are zeolites, which are tetrahedral-based aluminosilicates with well-defined three-dimensional framework structures. The pore openings of zeolites range from 5 to 15 Å.

Similar to zeolites, manganese oxides with tunnel structures exhibit molecular sieving properties[1,2] and are referred to as manganese oxide octahedral molecular sieves (OMS),[2−8] which include synthetic todorokite (OMS-1) and cryptomelane (OMS-2). Manganese oxide octahedra (MnO_6) are the basic structural units of OMS materials that combine to form tunnels on the order of 4.6 to 6.9 Å by linkage at their edges and vertexes. OMS-1 utilizes three MnO_6 octahedra on each side to form a 3 × 3 square tunnel with a pore size of about 6.9 Å. Similarly, OMS-2 has a 2 × 2 square tunnel with a pore size of about 4.6 Å. The smaller pore opening is probably the cause of the higher stability of OMS-2. In addition, countercations (e.g., K^+, Na^+, Ba^{2+}, and other alkali and alkaline earth metal ions) and water are present in the tunnels of OMS-1 and OMS-2 materials to provide charge balance and to stabilize the structure.

Mixed valency in mixed metal oxides is important for electron transport in chemistry. For example, the effectiveness of metal oxides for serving as catalysts for redox reactions, as electrode materials for electrochemical processes, and as chemical sensors for reductive gases are usually governed by their ability and tendency to cycle between different valence states of relevant cations and the mobility of oxygen ions.[9] From this standpoint, OMS materials have distinct advantages over aluminosilicate molecular sieve materials for applications in redox catalysis, batteries, and chemical sensors because of mixed manganese valencies (mainly, 4+, 3+, or 2+). However, the syntheses, characterization, and structural stability of OMS materials can be much more complicated than those of the oxides of main

* To whom correspondence should be addressed.
[†] University of Connecticut.
[‡] Current address: The Gillette Company, North Atlantic Group, One Gillette Park, Boston, MA 02127-1096.
[§] Texaco Research Center.

(1) Clearfield, A. *Chem. Rev.* **1988**, *88*, 125.
(2) Shen, Y. F.; Zerger, R. P.; DeGuzman, R. N.; Suib, S. L.; McCurdy, L.; Potter, D. I.; O'Young, C. L. *Science* **1993**, *260*, 511.
(3) Shen, Y. F.; Suib, S. L.; O'Young, C. L. *J. Am. Chem. Soc.* **1994**, *116*, 11020.
(4) DeGuzman, R. N. M.S. Thesis, The University of Connecticut, 1994
(5) DeGuzman, R. N.; Shen, Y. F.; Suib, S. L.; Shaw, B. R.; O'Young, C. L. *Chem. Mater.* **1993**, *5*, 1395.
(6) DeGuzman, R. N.; Shen, Y. F.; Neth, E. J.; Suib, S. L.; O'Young, C. L.; Levine, S.; Newsam, M. *Chem. Mater.* **1994**, *6*, 815.
(7) Shen, Y. F.; Zerger, R. P.; DeGuzman, R. N.; Suib, S. L.; McCurdy, L.; Potter, D. I.; O'Young, C. L. *J. Chem. Soc., Chem. Commun.* **1992**, 1213.
(8) Suib, S. L.; Iton, L. E. *Chem. Mater.* **1994**, *6*, 429.
(9) Yin, Y. G.; Xu, W. Q.; Suib, S. L. *Inorg. Chem.* **1995**, *34*, 4187.

10.1021/cm000868o CCC: $22.00
Published on Web 01/11/2002

group metals because of the multitude of different coordination numbers and oxidation states.

OMS-2 materials can be produced from birnessite, one kind of layered manganese oxides, by thermal and hydrothermal methods.[4,10−13] The oxidation of Mn^{2+} by oxidants, such as $KMnO_4$, $K_2S_2O_8$, and O_2, in acidic media has also been employed for the preparation of the synthetic cryptomelane.[4,14−18] Recently, sol−gel routes have been successfully applied to synthesize OMS-2 materials with a dilute reaction between $KMnO_4$ and fumaric acid.[19,20]

OMS-2 materials produced by reflux methods[4] after the oxidation of Mn^{2+} by $KMnO_4$ in acidic media have higher surface areas, smaller particle sizes, more acid sites, and more defects (primarily oxygen vacancies) than materials reported by others.[21] To alter electronic, catalytic, and structural properties of OMS-2 materials, some metal ions (such as Cu^{2+}, Zn^{2+}, and other divalent cations) other than alkaline metals have been successfully incorporated into OMS-2 materials as metal dopants. The selection of Cu^{2+}, Zn^{2+}, and other divalent cations is determined by their sizes, charges, and polarizabilities, which are similar to those of Mn^{2+}, to substitute for Mn^{2+} ions in the framework of OMS-2. Metal (M) doped OMS-2 materials, along with undoped OMS-2 materials, are referred to as M−OMS-2 materials in this work. Shen and DeGuzman et al.[3−7] have made extensive studies on the synthesis and characterization of M−OMS-2 materials. It has been observed that there is no significant difference among the Mn oxidation states for different M−OMS-2 materials prepared by reflux methods because the amount of cations, like Cu^{2+}, that can be incorporated into OMS-2 by reflux methods is diminutive.[22] The manganese oxidation states for OMS-2 and Cu−OMS-2 materials are always about 3.8,[6] which suggests that the majority of manganese is Mn^{4+} and only a small amount of Mn^{3+}/Mn^{2+} exists. The prepared M−OMS-2 materials have broad X-ray diffraction (XRD) peaks associated with small crystallite sizes (about 250 Å).

The synthesis, characterization, and potential applications of OMS materials have been reported in the literature.[2−9,21−26] Most literature focuses on the description of the materials themselves while fewer attempts have been made in the area of catalytic applications of OMS materials. Recently, we have systematically studied the catalytic performance of M−OMS-2 materials in the reaction of 2-propanol decomposition with relation to their surface and structural properties to explore the uniqueness and potential catalytic applications of these materials.[27] This paper focuses on detailed characterization of surface and structural properties of M−OMS-2 materials, especially studies on their elemental compositions, textural properties, and surface acid−base properties.

Although the syntheses and characterization of M−OMS-2 materials have been reported in the literature,[2−9,21−26] some new aspects are illustrated in this paper. The comprehensive elemental analysis results and discussion for M−OMS-2 materials shed light on the distribution of doped metal cations in the cryptomelane structure. The detailed phase transformations from cryptomelane to hausmannite or bixbyite and meantime, the evolution of O_2 were observed when M−OMS-2 materials were heated above their stable temperatures in thermal stability studies. Comprehensive N_2 sorption analyses confirmed that M−OMS-2 materials are porous materials, which contain micropores and mesopores, with total BET surface areas in the range of 70−110 m^2/g. TPD of adsorbed NH_3 or CO_2 revealed that all pretreated M−OMS-2 materials have similar acidity and basicity.

II. Experiments

2.1. Synthesis of M−OMS-2 Materials. OMS-2 was prepared by using reflux methods for the oxidation of Mn^{2+} by potassium permanganate. To prepare M−OMS-2 materials, metal (M) cations (Cu^{2+}, Zn^{2+}, Ni^{2+}, Co^{2+}, Al^{3+}, or Mg^{2+}) were doped into the OMS-2 structure with an a priori incorporation method, that is, adding aqueous solutions of dopant before refluxing to form the OMS-2 structure. The details of these preparations are given in the literature.[4]

2.2. Characterization of M−OMS-2 Materials. *2.2.1. Crystal Phase Identification by XRD.* The crystal phase identification of M−OMS-2 materials was carried out by collecting X-ray diffraction (XRD) patterns of fine powder samples using a Scintag 2000 XDS diffractometer with CuKα X-ray radiation. A 0.02 step in 2θ/count, beam voltage of 45 kV, and beam current of 40 mA were used. JCPDS powder diffraction data files were employed as references for crystal phase identification of samples.

2.2.2. Elemental Composition Analyses. Elemental compositions for potassium, manganese, and other metal cations of M−OMS-2 materials were analyzed with inductively coupled plasma−atomic emission spectroscopy (ICP−AES). The analyses were done at the Environmental Research Institute, Storrs, Connecticut, with a Perkin−Elmer 7−40 instrument equipped with an autosampler.

2.2.3. Morphology. The morphologies of M−OMS-2 materials were checked with scanning electron microscopy (SEM). SEM micrographs were taken in an Amray 1645 Scanning Electron Microscopy. Sample powders were spread uniformly on carbon paste on an aluminum sample holder to prepare samples for the SEM analysis.

2.2.4. Thermal Stability. Thermal stability of M−OMS-2 materials was studied with thermogravimetric analysis (TGA)

(10) Giovanoli, R.; Balmer, B. *Chimia* **1981**, *35*, 53.
(11) Giovanoli, R.; Faller, M. *Chimia* **1989**, *43*, 54.
(12) Golden, D. C.; Dixon, J. B.; Chen, C. C. *Clays Clay Miner.* **1986**, *34*, 511.
(13) Chen, C. C.; Golden, D. C.; Dixon, J. B. *Clays Clay Miner.* **1986**, *34*.
(14) Hypolito, R.; Valarelli, J. V.; Giovanoli, R.; Netto, S. M. *Chimia* **1984**, *38*, 427.
(15) Strobel, P.; Charenton, J. C. *Rev. Chim. Miner.* **1986**, *23*, 125.
(16) Parida, K. M.; Kanungo, S. B.; Sant, B. R. *Electrochim. Acta* **1981**, *26*, 435.
(17) Ambrose, J.; Covington, A. K.; Thirsk, H. R. *Power Sources* **1970**, *2*, 303.
(18) Feng, Q.; Kanoh, H.; Miyai, Y.; Ooi, K. *Chem. Mater.* **1995**, *7*, 148.
(19) Ching, S.; Roark, J. L.; Duan, N. G.; Suib, S. L. *Chem. Mater.* **1997**, *9*, 750.
(20) Duan, N. G.; Suib, S. L.; O'Young, C. L. *J. Chem. Soc., Chem. Commun.* **1995**, *13*, 1367.
(21) Suib, S. L. *Annu. Rev. Mater. Sci.* **1996**, *26*, 135.
(22) Tolentino, E. N.; Tian, Z. R.; Zhou, H.; Xia, G. G.; Suib, S. L. *Chem. Mater.* **1999**, *11*, 1733.
(23) Xia, G. G.; Yin, Y. G.; Willis, W. S.; Wang, J. Y.; Suib, S. L. *J. Catal.* **1999**, *185*, 91.
(24) Yin, Y. G.; Xu, W. Q.; DeGuzman, R.; Suib, S. L.; O'Young, C. L. *Inorg. Chem.* **1994**, *33*, 4384.
(25) Yin, Y. G.; Xu, W. Q.; DeGuzman, R.; Shen, Y. F.; Suib, S. L.; O'Young, C. L. In *Zeolites and Related Microprous Materials: State of the Art 1994*; Weitamp, J., Karge, H. G., Pfeifer, H., Holderich, W., Eds.; Elsevier Science B. V.: Amsterdam, 1994; Vol. 84, p 453.
(26) O'Young, C. L.; Sawicki, R. A.; Suib, S. L. *Microporous Mater.* **1997**, *11*, 1.
(27) Chen, X.; Shen, Y. F.; Suib, S. L.; O'Young, C. L. *J. Catal.* **2001**, *197*, 292.

Table 1. ICP−AES Elemental Analysis Results and Average Crystallite Sizes of Cu−OMS-2 Materials

materials	Cu−OMS-2-I	Cu−OMS-2-II	Cu−OMS-2-III	Cu−OMS-2-IV	OMS-2
Cu[a] (mol/100 g[b])	0.056	0.050	0.041	0.018	0
K[a] (mol/100 g[b])	0.086	0.093	0.099	0.115	0.115
Mn[a] (mol/100 g[b])	1.133	1.106	1.120	1.148	1.300
Mn/K[a] (molar ratio)	13.20	11.86	11.27	10.02	11.30
Cu/K[c] (molar ratio)	1.78	0.89	0.42	0.07	0
Cu/K[a] (molar ratio)	0.65	0.54	0.41	0.16	0
Cu/Mn[a] (molar ratio)	0.049	0.045	0.036	0.016	0
τ[d] (Å)	160	180	200	230	280

[a] The calculated results from ICP−AES data. [b] With respect to 100 g material. [c] The initial Cu/K molar ratio in the reactants. The initial molar ratio of Mn/K was 2.39. [d] Average crystallite sizes calculated from the Scherrer equation.

Table 2. ICP−AES Elemental Analysis Results and Average Crystallite Sizes of M−OMS-2 Materials

M	OMS-2	Mg	Ni	Al	Zn	Cu[a]	Co
M[b] (mol/100 g[c])	0	0.005	0.017	0.022	0.023	0.056	0.085
K[b] (mol/100 g[c])	0.115	0.105	0.100	0.099	0.098	0.086	0.098
Mn[b] (mol/100 g[c])	1.300	0.945	0.910	0.949	0.917	1.133	0.874
Mn/K[b] (molar ratio)	11.30	9.00	9.09	9.61	9.40	13.20	8.88
M/K[b] (molar ratio)	0	0.05	0.17	0.22	0.24	0.65	0.86
M/Mn[b] (molar ratio)	0	0.005	0.019	0.023	0.025	0.049	0.097
τ[d] (Å)	280	210	230	200	210	160	160

[a] Refers to Cu−OMS-2-I. [b] The calculated results from ICP−AES analysis. The initial Mn/K and M/K molar ratios in the reactants were 2.39 and 1.78, respectively. [c] With respect to 100 g material. [d] Average crystallite sizes calculated with the Scherrer equation.

using a DuPont 951 TGA system. About 10 mg of sample powder was loaded into a platinum sample holder for TGA. Both N_2 [UHP (ultrahigh purity) grade] and O_2 (UHP) were used as carrier gases for TGA experiments, and the flow rate of the gases was about 30 mL/min. The ramping rate was set at 10 °C /min with scans from 30 to 900 °C.

The gas products evolved from OMS-2 during TGA experiments were determined with temperature-programmed desorption (TPD) experiments, which were carried out in the range of 30−700 °C with the same temperature ramp of 10 °C /min as in the TGA experiment. About 44 mg of OMS-2 was loaded into a quartz tubular reactor and put into a temperature-programmed furnace. A He or O_2 flow with a flow rate of 60 mL/min was used to provide the atmosphere and carry out the evolved gaseous products, which were monitored by mass spectrometry (MS) with an MKS−UTI PPT quadrupole residual gas analyzer. The peaks with *m*/*e* equal to 2, 18, 32, and 44 were chosen to monitor the evolution of H_2, H_2O, O_2, and CO_2, respectively, according to their MS cracking patterns and on the basis of high intensity and little interference.

To monitor the crystal phase of OMS-2 at different temperatures during the TPD experiments, XRD patterns were collected at room temperature for the quickly cooled OMS-2 materials after the temperature program was stopped at certain temperatures (500, 600, or 700 °C).

2.2.5. Textural Properties. Textural properties, such as surface area and pore size distribution of tested materials, were studied with a Micromeritics ASAP 2010 System. Before acquiring nitrogen adsorption and desorption isotherms at 77 K, samples were outgassed at 300 °C under vacuum for 12 h.

Surface areas were determined by nitrogen adsorption data, with Brunauer−Emmett−Teller (BET) methods.[28] The relative pressure p/p_0 (p and p_0 are the pressures of N_2 vapor at adsorption and its saturation vapor pressure at 77 K, respectively) used for the calculation is in the range of 0−0.3.

2.2.6. Acid−Base Properties. The acidic and basic properties of M−OMS-2 materials were studied with the TPD of NH_3 and CO_2, respectively. Before adsorption, 44 mg of samples having a particle size of 28−48 mesh (300−590 μm) were pretreated in a He stream (60 mL/min) at 300 °C for 1 h to desorb adsorbed H_2O, air, and other impurities. NH_3 or CO_2 was introduced with a flow (60 mL/min) of 0.5 mol % NH_3/He or 10 mol % CO_2/He, respectively, for one half hour at 22 °C. A continuous He flow was then applied to purge unabsorbed or weakly adsorbed NH_3 or CO_2 for about 3 h until the MS signals for NH_3 or CO_2 leveled off. The evolution of NH_3 or CO_2, between 22 and 700 °C with a heating rate of 10 °C /min, was monitored by MS. The peaks with *m*/*e* equal to 15 and 44 were chosen to monitor the evolution of NH_3 and CO_2, respectively, according to the MS cracking patterns of all possible desorbed gases (NH_3, CO_2, H_2, H_2O, O_2, and CO_2) and on the basis of high intensity and little interference.

III. Results

3.1. XRD Study. XRD pattern for fresh OMS-2 is shown as pattern a in Figure 3, corresponding to synthetic cryptomelane (KMn_8O_{16}, JCPDS 29, 1020). All other synthesized M−OMS-2 samples have XRD patterns similar to OMS-2. This indicates that all synthesized M−OMS-2 materials have a cryptomelane type structure.

In general, the peaks in the XRD patterns for OMS-2 and all M−OMS-2 materials are broad as shown in the pattern a in Figure 3. The average crystallite sizes of all materials can be calculated from the Scherrer equation[29] using the strongest peak ($2\theta = 38°$) and are listed in Tables 1 and 2. The average crystallite sizes of Cu−OMS-2 materials decrease with increasing Cu dopant content and all M−OMS-2 materials show the same trend (except for Mg−OMS-2) even with different kinds of metal dopants, as shown in Tables 1 and 2.

3.2. ICP−AES Elemental Analysis. The results of ICP−AES elemental analyses for cations in all synthesized M−OMS-2 materials are shown in Tables 1 and 2. The Mn/K molar ratio increased significantly from initially 2.39 in the reactants to around 9−13 in the prepared materials. These data suggest that a lot of potassium ions were washed out during the syntheses. The M/K molar ratios decreased from the original synthesis ratios to the final ratios in the prepared materials, except for Cu−OMS-2-III and -IV where smaller Cu/K molar ratios were used for synthesis. This indicates that even more of the metal dopant was washed out during the synthesis.

Although the initial molar content of metal cation and M/K molar ratios (1.79) in the reactants were the same

(28) Brunauer, S.; Emmett, P. H.; Teller, E. *J. Am. Chem. Soc.* **1938**, 309.

(29) West, A. R. *Solid State Chemistry and its Applications*; John Wiley & Sons Ltd.: Chichester, 1984; p 174.

in the syntheses of different metal doped M−OMS-2 materials, the final doped M content and M/K molar ratios in prepared materials are different from each other. This is probably because different metal cation dopants have different physical and chemical properties that affect the content of substituted cations during synthesis. Under the same synthesis conditions, the doped metal content increases in the order $Mg^{2+} < Ni^{2+} \sim Al^{3+} \sim Zn^{2+} < Cu^{2+} < Co^{2+}$. The final Cu/K molar ratios in prepared Cu−OMS-2 materials decreased with the initial Cu/K molar ratios in the reactants. This indicates that the final M/K molar ratios in the prepared materials can be increased or decreased with either increasing or decreasing, respectively, the initial M/K molar ratios in the reactants.

According to Table 1, when the Cu^{2+} ion content increases from 0 in OMS-2 to 0.018 mol/100 g of material in Cu−OMS-2-IV, the Mn content decreases from 1.300 mol/100 g of material in OMS-2 to 1.148 mol/100 g of material in Cu−OMS-2-IV. However, the K^+ content does not change. With a further increase of Cu^{2+} content, the Mn content does not change much more, but the K^+ content decreases constantly. This suggests that Cu^{2+} ions at first mostly substitute for some manganese ions in the framework of OMS-2 but not for K^+ ions in the tunnel sites of OMS-2. However, Cu^{2+} ions probably begin to substitute for some K^+ ions in the tunnel sites if more Cu^{2+} ions are doped in during the synthesis. This is also supported by the fact that the ratios of Mn/K and Cu/K in the prepared Cu−OMS-2 materials increase rapidly while the Cu/Mn ratio grows much slower with increasing Cu content after it reaches 0.041 mol/100 g of sample.

This trend is also indicated in Table 2, after M ions are doped into OMS-2 materials during preparation. The number of moles of potassium ions in 100 g of material decreases slightly from 0.115 in OMS-2 to about 0.100 in other M−OMS-2 materials. However, the number of moles of manganese ions in 100 g of material decreases from 1.300 in OMS-2 to 0.87−1.15 in other M−OMS-2 materials. Therefore, in M−OMS-2 materials, most of the M cations are probably in the framework of OMS-2 because of the substitution of manganese ions. This is consistent with the general assumption that the transition metal cations mostly reside in the framework of the cryptomelane structure for the M−OMS-2 materials prepared with a priori incorporation.[23]

Interestingly, the Mn content in Cu−OMS-2 materials is generally higher than those in other metal cation doped M−OMS-2 materials, as indicated in Tables 1 and 2, suggesting that more Cu^{2+} ions are in tunnels by substituting for K^+, especially when the Cu^{2+} content is relatively high (e.g., for Cu−OMS-2-I, -II, -III). This is also supported by the fact that the Mn/K molar ratios in Cu−OMS-2 materials are in the range of 10−12, which are generally higher than those (in the range of 8.9−10) for other metal cation doped M−OMS-2 materials.

3.3. Morphology. Figure 1 reveals the typical fibrous morphology of the prepared OMS-2 materials. The maximum diameter of the fibrous OMS-2 material is approximately 0.2 μm. Similar fibrous morphology was observed for metal ion doped M−OMS-2 materials. This is consistent with previous results[4,6] for M−OMS-2 materials prepared by reflux methods.

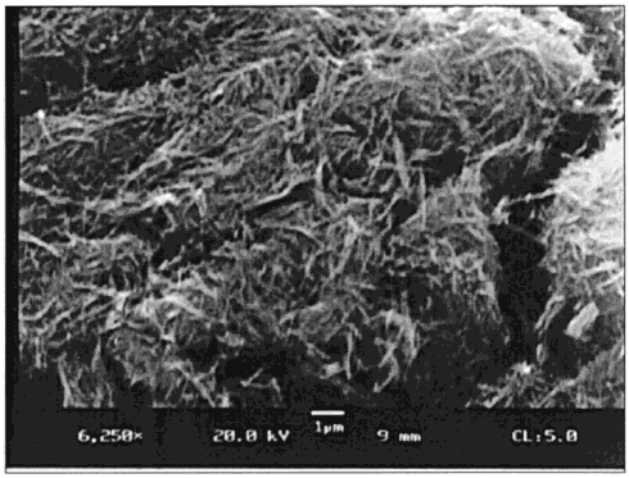

Figure 1. Morphology of OMS-2 revealed by SEM.

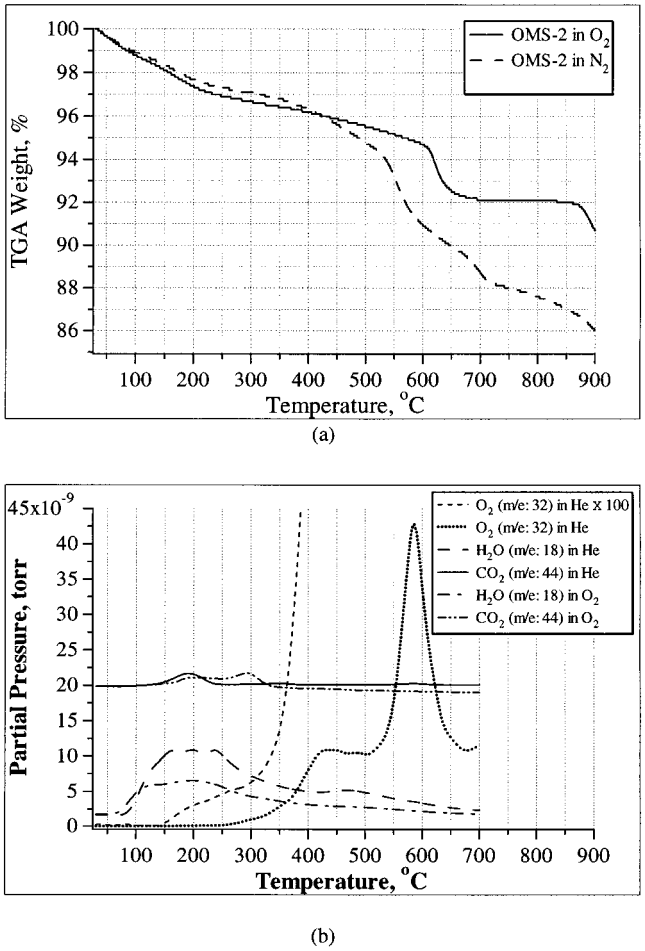

Figure 2. TGA (a) and TPD (b) plots for OMS-2 in both N_2/He and O_2 atmospheres (30 to 700 or 900 °C with a ramp of 10 °C/min).

3.4. Thermal Stability. Thermal stability of M−OMS-2 materials was studied with thermogravimetric analysis (TGA) both in N_2 and O_2 atmospheres in the range of 30−900 °C with a ramping rate of 10 °C/min. All prepared M−OMS-2 materials show similar thermal stabilities, which are summarized in Figures 1, 5, and 6.

Figure 2a shows TGA results for OMS-2 in both N_2 and O_2 atmospheres. The results indicate that OMS-2 is more thermally stable in O_2 than in N_2 atmosphere.

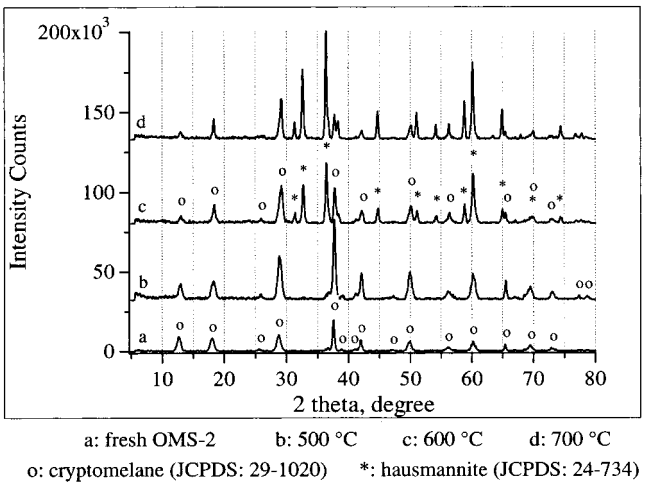

Figure 3. XRD patterns of OMS-2 before and after TPD experiments in He atmosphere at different temperatures.

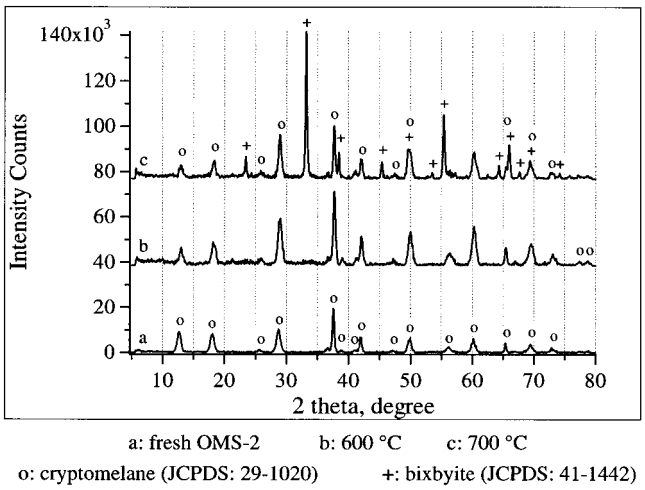

Figure 4. XRD patterns of OMS-2 before and after TPD experiments in O_2 atmosphere at different temperatures.

This is consistent with our previous results for M−OMS-2 materials.[6,22]

Figure 2b indicates the evolution of O_2, H_2O, and CO_2 from OMS-2 during thermal treatment under He or O_2 streams for TPD experiments in the range of 30−700 °C with the same temperature ramp of 10 °C/min as TGA experiments. The small amount of CO_2 evolution during thermal treatment is probably due to ambient CO_2 adsorbed on OMS-2 material in air. The He atmosphere, which was used in the TPD experiments, should be similar to N_2 in TGA experiments because both He and N_2 are inert gases for OMS-2 materials.

Combining TGA and TPD (Figure 2) data leads to a 3% weight loss of OMS-2 between 30 and 300 °C, which is due to the evolution of H_2O and CO_2. Further dehydration and O_2 loss start at 300 °C and lead to a 2% weight loss in the range of 300−500 °C. The large peak for O_2 around 580 °C contributes to a 6% weight loss in the range of 500−700 °C.

In O_2 atmosphere, the evolution of H_2O and CO_2 from OMS-2 in the range of 30−350 °C was also observed and gives rise to a 4% weight loss. Further weight loss between 350 and 700 °C is about 4%, which is less than 7% in N_2 atmosphere. This may be due to less O_2 loss from OMS-2 in O_2 than in N_2/He atmosphere.

The crystal phase change of OMS-2 during TPD experiments was observed with XRD for fresh OMS-2 and OMS-2 samples used in TPD experiments. Figures 3 and 4 display XRD patterns of OMS-2 before and during TPD experiments in He and O_2 atmospheres, respectively.

As shown in Figures 3 and 4, OMS-2 is stable up to about 500 °C and is gradually transformed into hausmannite in He atmosphere. In O_2 atmosphere, OMS-2 is stable up to a higher temperature of 600 °C and is progressively converted into bixbyite. This is also consistent with our previous results for M−OMS-2 materials.[6,22]

Figure 5 summarizes TGA profiles for Cu−OMS-2 materials with different Cu dopant content in N_2 and O_2 atmospheres. Cu−OMS-2 materials with different Cu^{2+} dopant content have thermal stabilities similar to that of OMS-2, although the weight losses seem to escalate with increasing Cu^{2+} dopant concentration. The first weight loss temperatures T_1 and T_1', in N_2 and O_2

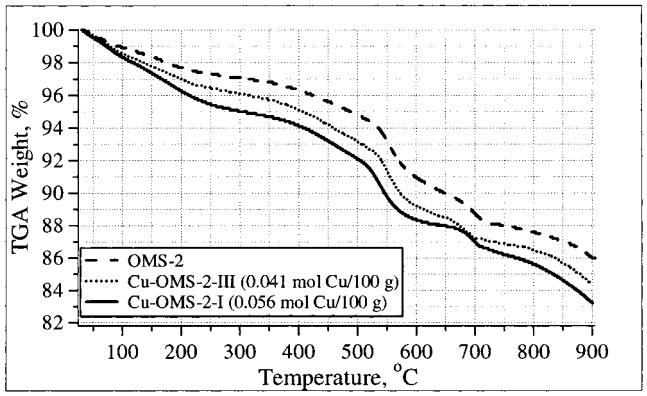

(a)

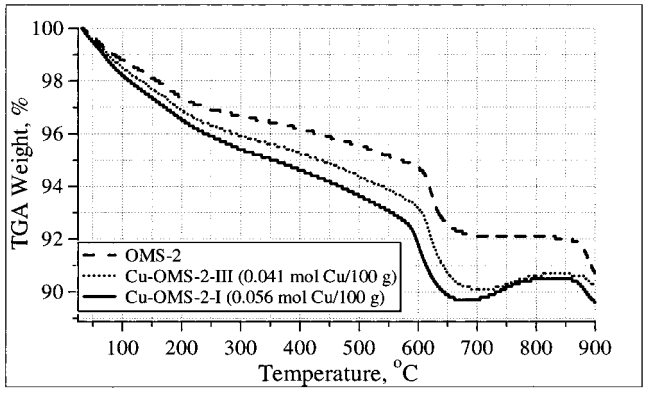

(b)

Figure 5. TGA plots for Cu−OMS-2 with different Cu content in (a) N_2 atmosphere and (b) O_2 atmosphere.

atmospheres, respectively, decrease when Cu^{2+} dopant concentrations increase. These data suggest that Cu−OMS-2 materials become less thermally stable with increasing Cu^{2+} dopant content.

The M−OMS-2 materials with different M dopants also exhibit similar thermal stabilities as OMS-2 material although there are small differences from one to the other, as illustrated in Figure 5. The weight losses seem to increase with increasing M dopant in both N_2 and O_2 atmospheres, although Al−OMS-2 has the slightly higher first and second weight loss temperatures (T_1 and T_2) in N_2 atmosphere. This indicates that metal cation

Table 3. Surface Textural Properties of Fresh M−OMS-2 Materials

		surface area, m^2/g			pore volume, cm^3/g				pore size, Å	
sample	M[a] mol/ 100 g	S_{mic}[b]	S_{ext}[c]	S_{BET}[d]	V_{mic}[e]	V_{mes}[f]	V_{mac}[g]	V_t[h]	micro[i]	meso[j]
OMS-2	0	10.8	60.8	71.6	0.0052	0.139	0.085	0.229	5	250
Cu−OMS-2-IV	0.018	12.9	65.3	78.3	0.0062	0.168	0.212	0.386	5	300
Cu−OMS-2-III	0.041	18.8	76.7	95.5	0.0092	0.198	0.131	0.338	5	350
Cu−OMS-2-II	0.05	14.5	73.6	88.1	0.0070	0.181	0.173	0.361	5	400
Cu−OMS-2-I	0.056	19.1	78.7	97.8	0.0093	0.220	0.184	0.413	5	350
Mg−OMS-2	0.005	12.5	68.2	80.8	0.0060	0.169	0.158	0.333	5	350
Ni−OMS-2	0.017	13.4	69.9	83.3	0.0065	0.175	0.164	0.346	5	300
Al−OMS-2	0.022	15.5	71.0	86.4	0.0076	0.181	0.116	0.305	5	300
Zn−OMS-2	0.023	12.7	69.2	82.0	0.0061	0.174	0.186	0.366	5	400
Co−OMS-2	0.085	16.1	90.2	106.3	0.0077	0.310	0.192	0.510	5	300

[a] Metal dopant (other than K) content in 100 g material. [b] Surface area due to micropores in a sample, obtained by subtraction of S_{BET} with S_{ext}. [c] Surface area due to external surface in a sample, calculated using t-plot methods. [d] Total surface area of a sample, calculated with BET methods. [e] Micropore (<20 Å) volume based on t-plot methods. [f] Mesopore volume (20−500 Å) based on BJH methods. [g] Macropore (500−3000 Å) volume based on BJH methods. [h] Total pore volume obtained by the sum of V_{mic}, V_{mes}, and V_{mac}. [i] The most probable micropore size based on HK methods. [j] The most probable mesopore size based on BJH methods.

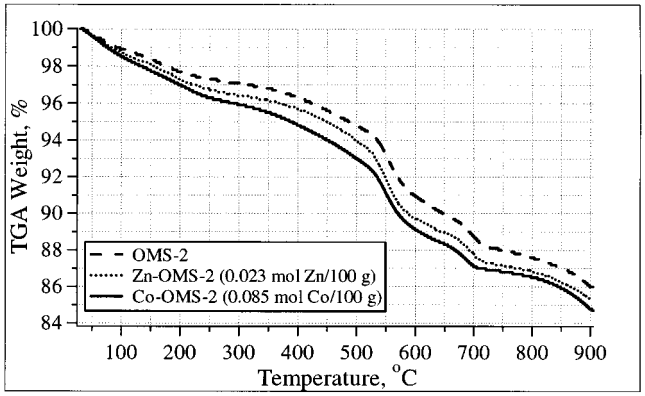

(a)

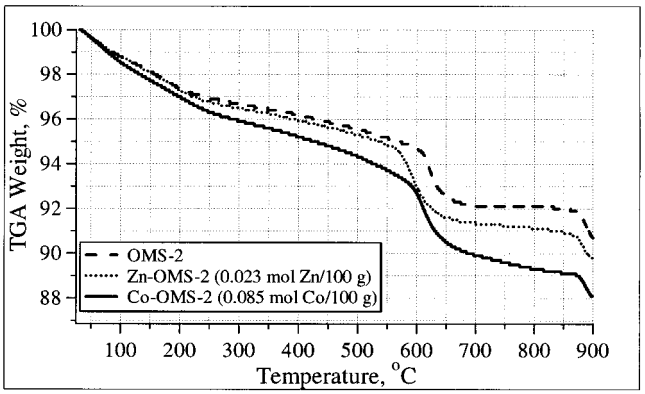

(b)

Figure 6. TGA plots for M−OMS-2 materials in (a) N_2 atmosphere and (b) O_2 atmosphere.

doped M−OMS-2 materials have similar but slightly lower thermal stabilities than undoped OMS-2, especially when the dopant content is relatively high.

3.5. Textural Properties. The N_2 adsorption isotherm on OMS-2 is shown in Figure 7. Type II adsorption isotherms with micropore filling at low p/p_0 and capillary condensation at high p/p_0 are observed. At low p/p_0, micropore filling of Type I adsorption isotherm occurs, indicating the existence of micropores in OMS-2. A hysteresis loop of Type B, according to the de Boer's classification[30] of types of hysteresis loops (Type B corresponding to Type H3, according to IUPAC[31]), occurs at high p/p_0 close to saturation, suggesting the existence

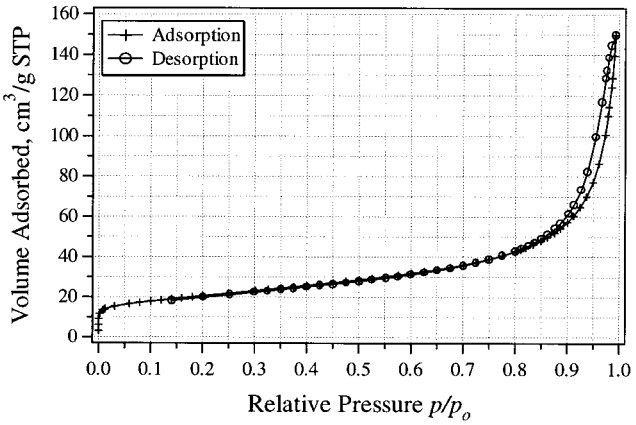

Figure 7. N_2 adsorption isotherm for OMS-2 at 77 K.

of slit-shaped mesopores with nonuniform sizes or shapes[32] in OMS-2. Other prepared M−OMS-2 materials have adsorption isotherms of N_2 similar to OMS-2. This indicates that all prepared M−OMS-2 materials have similar textural properties, which are summarized in Table 3.

According to Table 3, M−OMS-2 materials are porous and have surface areas around 70−110 m^2/g, in which about 20% are due to micropores in the sample. The pores in M−OMS-2 materials are comprised of micropores, which contribute 2% of total pore (up to 3000 Å) volume; mesopores, which contribute 54%; and macropores (500−3000 Å), which contribute 44%. The most probable pore size in the micropore range is around 5 Å and in the mesopore range is around 350 Å for M−OMS-2 materials. Compared to OMS-2, metal cation doped M−OMS-2 materials have larger most probable mesopore sizes (300−400 Å, compared to 250 Å) and slightly higher surface areas and pore volumes.

3.6. Surface Basicity. TPD of CO_2 was applied to a study of the basicity of M−OMS-2 materials. In TPD of adsorbed CO_2, the strength and amount of basic sites are reflected in the temperature at which the CO_2 desorption peak appears and the area of the peak, respectively.

(30) de Boer, J. H. In *The Structure and Properties of Porous Materials*; Everett, D. H., Stone, F. S., Eds.; Butterworth: London, 1958; p 68.
(31) Gregg, S. J.; Sing, K. S. W. *Adsorption, Surface Area and Porosity*, 2nd ed.; Academic Press Inc.: London, 1982.
(32) Leofanti, G.; Padovan, M.; Tozzola, G.; Venturelli, B. *Catal. Today* **1998**, *41*, 207.

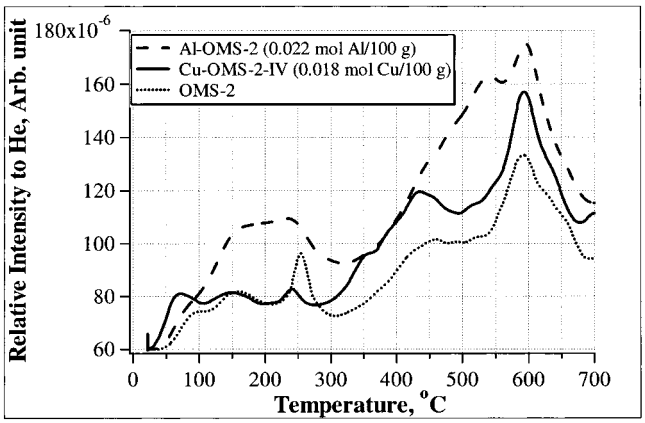

Figure 8. TPD plots of CO_2 desorbed from M−OMS-2 materials (20−700 °C with a ramp of 10 °C/min).

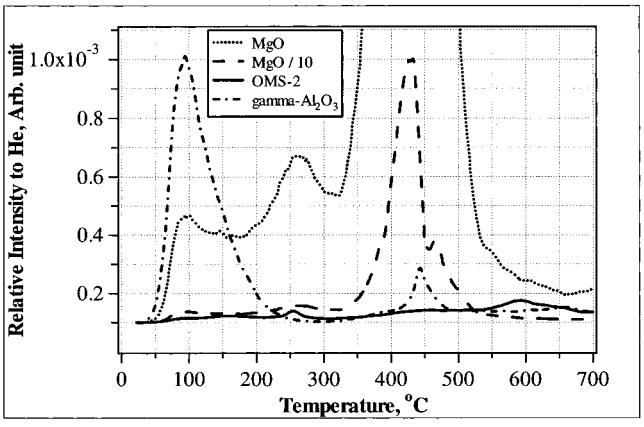

Figure 9. TPD plots of CO_2 desorbed from OMS-2 and MgO (20−700 °C with a ramp of 10 °C/min).

Figure 8 shows TPD plots of CO_2 desorbed from M−OMS-2 in the range of 20−700 °C with a temperature ramp of 10 °C/min. All M−OMS-2 materials show similar TPD profiles of CO_2, which indicate that they have weak basic sites (WBS, corresponding to the peaks between 100 and 300 °C), moderate basic sites (MBS: 300−500 °C), and strong basic sites (SBS: 500−700 °C). There are no particular temperature cutoffs or protocols for the strength regimes of basic sites. The number of WBS that can retain CO_2 increases in the order Cu−OMS-2-IV ∼ OMS-2 < Al−OMS-2. However, the number of MBS and SBS increase in the order OMS-2 < Cu−OMS-2-IV < Al−OMS-2. Undoped OMS-2 has some unique basic sites corresponding to a sharp peak at about 250 °C.

Although M−OMS-2 materials have some basic sites of different strengths on their surface after the pretreatment in He at 300 °C for 1 h, the amounts of basic sites on M−OMS-2 materials are much smaller than on MgO, which also has a large amount of basic sites with varied strengths, as shown in Figure 9. Interestingly, the TPD plot of CO_2 adsorbed on γ-Al_2O_3 in Figure 9 indicates that there are more very weak basic sites (VWBS: corresponding to the sharp peak at about 100 °C) on the surface of γ-Al_2O_3 than on MgO and some MBS, whose amount is greater than those on M−OMS-2 materials but much less than that on MgO. However, the amount of SBS on γ-Al_2O_3 is less than those on M−OMS-2 materials.

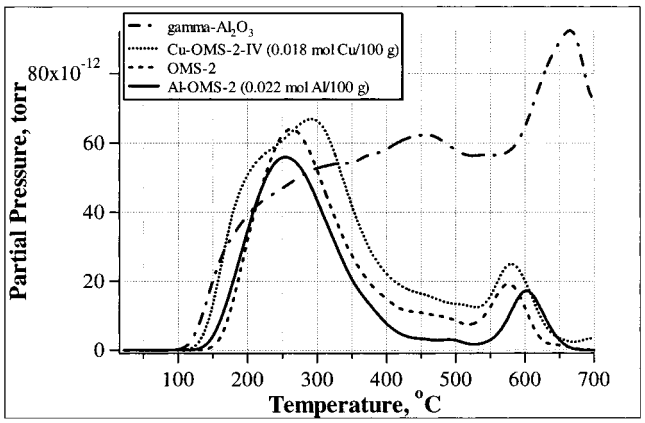

Figure 10. TPD plots of NH_3 desorbed from M−OMS-2 materials and γ-Al_2O_3 (20−700 °C with a ramp of 10 °C/min).

3.7. Surface Acidity. TPD of NH_3 was used to study the acidity of M−OMS-2 materials. Figure 10 shows TPD plots of NH_3 desorbed from M−OMS-2 materials and γ-Al_2O_3 in the range of 20−700 °C with a ramp of 10 °C/min. All M−OMS-2 materials give similar results showing that they have a lot of weak acid sites, as indicated by the peaks around 250−300 °C, and some strong acid sites, as indicated by the peaks around 600 °C, after being pretreated in He at 300 °C for 1 h. The strength of weak acid sites is in the increasing order of Al−OMS-2 < OMS-2 < Cu−OMS-2-IV, and the strength of strong acid sites is in the order of Cu−OMS-2-IV ∼ OMS-2 < Al−OMS-2. Compared to γ-Al_2O_3, the strength and the amounts of strong acid sites on M−OMS-2 surfaces are weaker and smaller, respectively.

IV. Discussion

XRD patterns confirmed that M−OMS-2 materials have a cryptomelane structure, which contains a well-defined 2 × 2 tunnel structure having a pore size of about 4.6 Å and is composed of double chains of edge-shared MnO_6 octahedra and corner-sharing of double chains.[4−6] The 2 × 2 tunnel structure needs some large ions, such as K^+ ion in the tunnels, to prevent collapse of the framework. The electron diffraction data for OMS-2 in the literature[6] also suggested that K^+ ions are primarily located in the tunnels of OMS-2. The tetragonal I^4/m symmetry of cryptomelane appears to be justified for OMS-2 by Rietveld refinement results, as well as electron and X-ray diffraction simulations.[6]

The ICP−AES elemental analysis results, as shown in Tables 1 and 2 for M−OMS-2 materials, suggested that most of the M cations are probably in the framework of OMS-2 because of the substitution of some manganese ions after doping of metal cations. Cu^{2+} ions mostly substitute for some manganese ions in the framework of OMS-2 when the Cu^{2+} ion content is small (like Cu−OMS-IV). Cu−OMS-2 materials are unique among M−OMS-2 materials because Cu−OMS-2 materials have more doped metal cations (Cu^{2+}) in tunnels by substituting for K^+, especially when the Cu^{2+} content is relatively high (e.g., Cu−OMS-2-I, -II, -III).

Clearly, a detailed structural study is needed to confirm the locations of the doped metal ions in the prepared M−OMS-2 materials, although the confirmation is often difficult because of the limited small amount of doped metal ions. Structural characterization

methods, such as electron paramagnetic resonance (EPR) measurements, X-ray photoelectron spectroscopy (XPS), X-ray absorption near edge spectroscopy (XANES), and extended X-ray absorption fine structure (EXAFS) measurements, may shed some light on the locations of the doped metal ions. As one reviewer strongly suggested, a detailed structural study on the prepared M−OMS-2 materials is being carried out in our group.

Under the same synthesis conditions, the doped metal content in the prepared M−OMS-2 materials increases in the order $Mg^{2+} < Ni^{2+} \sim Al^{3+} \sim Zn^{2+} < Cu^{2+} < Co^{2+}$ as shown in Table 2. This means that Cu^{2+} and Co^{2+} are more easily doped into the cryptomelane structure of OMS-2 than are other metal cations. Although Co−OMS-2 has a higher metal cation dopant content (Co^{2+}: 0.085 mol/100 g) than Cu−OMS-2-I (Cu^{2+}: 0.056 mol/100 g), the K^+ content in Co−OMS-2 is higher than that in Cu−OMS-2-I. Meanwhile, the manganese content in Co−OMS-2 is lower than that in Cu−OMS-2-I, indicating that more Cu^{2+} ions are in tunnels by substituting for K^+ in Cu−OMS-2-I than Co^{2+}, which has more occupied framework sites by substituting for manganese in Co−OMS-2. The higher probability of having Cu^{2+} in tunnel positions than Co^{2+} is probably because Cu^{2+} is not stable in the framework of cryptomelane because of distorted CuO_6 octahedra caused by Jahn−Teller distortions.

Generally, it is difficult to verify or quantify the substitution of Mn^{2+} with cations such as Cu^{2+} because the amount of Cu^{2+} that can be incorporated into OMS-2 by reflux methods is diminutive.[22] Applications of certain characterization methods, such as electron paramagnetic resonance (EPR) measurements, may provide some evidence indicating that cations such as Cu^{2+} substitute for Mn^{2+}. DeGuzman et al.[6] have found that incorporation of Cu^{2+} into OMS-2 materials diminishes saturation of Mn^{2+} and that the electron paramagnetic resonance (EPR) data of Cu−OMS-2 shows a characteristic six-line pattern of octahedral Mn^{2+} coordination. In OMS-2, Mn^{2+} is EPR silent because Mn^{2+} presents in higher concentration. The EPR data of Cu−OMS-2 also contains Cu^{2+} line that is superposed with Mn^{2+} line. The characteristics of the Cu^{2+} line suggest that Cu^{2+} is in a distorted octahedral environment in the OMS-2 structure. No unit cell change with the framework substitution for M−OMS-2 materials has been observed in our group.

The crystallization process of Cu−OMS-2 during synthesis is somewhat hindered by the doping of Cu^{2+}. After Cu^{2+} (up to 0.056 mol/100 g) was doped into OMS-2, Cu−OMS-2 materials still have the cryptomelane structure. However, with increasing Cu^{2+} content, the average crystallite size of cryptomelane decreases from 280 Å for OMS-2 to 160 Å for Cu−OMS-2-I. Meanwhile, TGA results suggest that Cu−OMS-2 materials become less thermally stable in both N_2 and O_2 atmospheres with increasing Cu^{2+} content.

TGA studies of M−OMS-2 materials in this research indicate that, as a general trend, the metal cation doped M−OMS-2 materials have similar but slightly lower thermal stability than undoped OMS-2, especially when the dopant content is relatively high. This trend was also observed by Tolentino et al. for Cu−OMS-2 materials.[22]

M−O bonding strengths in a sample of single or mixed metal oxide can be probed through the ease of oxygen release during TPD treatment of the sample. The TPD plot of O_2 from OMS-2 in He atmosphere shows mainly two peaks: one broad peak around 450 °C in a medium-temperature (MT) region (300−500 °C) and one sharp peak at around 580 °C in a high-temperature (HT) region (500−700 °C) with much higher intensity, as shown in Figure 2b. A much smaller and broader peak around 200 °C in a low-temperature (LT) region (100−300 °C), which can be seen as the enlarged line in Figure 2b, is also observed. Yin et al.[9,24,25] reported similar results for M−OMS-2 materials prepared by reflux methods and concluded that the effect of doping metal cations on the oxygen species in M−OMS-2 is generally insignificant. However, Cu−OMS-2 exhibits a distinct feature of more availability of reactive oxygen species at low-temperature range.

The TPD of O_2 from a typical transition-metal oxide catalyst can be generally divided into three peaks, which correspond to physisorbed O_2, chemisorbed oxygen (usually O^-), and lattice oxygen (O^{2-}), at progressively higher temperatures. Accordingly, the broad and very small LT peak around 200 °C of OMS-2 can be assigned to physisorbed O_2. The broad and small MT peak around 450 °C is probably due to weakly chemisorbed oxygen bound to Mn^{2+} ions,[33] which present in small amount in the framework of OMS-2 for maintaining electrical neutrality due to incorporation of tunnel cations. The sharp and big HT peak around 580 °C is probably due to lattice oxygen, which bound more strongly to Mn^{4+}. This assignment is also supported by XRD results, as shown in Figure 3. The initial cryptomelane phase of OMS-2 is stable up to about 500 °C, indicating that oxygen species released from OMS-2 below 500 °C are not from lattice oxygen but some physisorbed or chemisorbed oxygen. At 600 °C, some cryptomelane has transformed into hausmannite, verifying that release of some lattice oxygen started between 500 and 600 °C.

As far as we know, no systematic textural property studies of synthetic M−OMS-2 materials have been reported in the literature. O'Young et al. used argon adsorption isotherms to study the micropore size distribution of OMS-2.[26] A partial Type 1 isotherm, only up to a relative pressure of about 0.4, verifies the existence of micropores in OMS-2, but no full argon adsorption isotherm data were given.

The full nitrogen adsorption isotherms of the prepared M−OMS-2 materials in this research allow a more comprehensive pore analysis up to 3000 Å. HK methods were employed for micropore analysis and the BJH method was used for mesopore and macropore (up to 3000 Å) analysis. The analysis confirmed that M−OMS-2 materials are porous materials containing micropores, which contribute 2% of total pore (up to 3000 Å) volume; mesopores, which contribute 54%; and macropores (500−3000 Å), which contribute 44%. The most probable pore size in the micropore range is about 5 Å, which is close to the tunnel size of 4.6 Å for OMS-2, and in the mesopore range is around 350 Å for M−OMS-2 materials. Although only about 2% of total pore volume are

(33) Shannon, R. D.; Prewitt, C. T. *Acta Crystallogr.* **1969**, *25*, 925.

micropores in M−OMS-2 materials, about 20% of the total BET surface area (70−110 m^2/g) is contributed by micropores in the sample.

Compared to undoped OMS-2, metal cation doped M−OMS-2 materials have slightly higher surface areas and pore volumes, especially when the dopant content is relatively high. This is consistent with the XRD observation that doped M−OMS-2 materials generally have smaller average crystallite sizes of cryptomelane because of more defects introduced by metal cation dopants.

Basicity studies revealed that all M−OMS-2 materials prepared in this research have similar TPD profiles for CO_2 desorption. This means that all of these materials have similar patterns of different basic sites with varied strengths and amounts after pretreatment. Compared to MgO, which is commonly considered to be a solid base catalyst,[34−36] the relative strength and amount of basic sites on the surface of M−OMS-2 materials are weaker and fewer. There are more SBS but less VWBS and MBS on M−OMS-2 materials than on γ-Al_2O_3, which is generally considered to be an amphoteric oxide.

TPD studies of NH_3 adsorbed on pretreated M−OMS-2 materials provide evidence that all M−OMS-2 materials also have similar acidities. The relative strength and amount of acid sites on the surface of M−OMS-2 materials are generally weaker and fewer, as compared to γ-Al_2O_3.

V. Conclusions

Different metal cation (Cu^{2+}, Zn^{2+}, Ni^{2+}, Co^{2+}, Al^{3+}, or Mg^{2+}) doped M−OMS-2 materials were prepared with reflux methods. Prepared M−OMS-2 materials have a cryptomelane structure with a typical fibrous morphology, as confirmed by XRD and SEM studies.

The results of ICP−AES elemental analyses for M−OMS-2 materials suggest that most doped metal cations are probably in the framework of the cryptomelane structure, except for Cu^{2+} ions which are mostly in tunnels substituting for K^+, especially when the Cu^{2+} content is relatively high. Among metal cations employed in this research, more Cu^{2+} and Co^{2+} can be doped into the cryptomelane structure of OMS-2 under similar synthesis conditions.

M−OMS-2 materials are more thermally stable in O_2 than in inert (N_2 or He) atmospheres, as shown by TGA and XRD studies. OMS-2 is stable up to about 500 °C and is gradually transformed into hausmannite in He atmosphere. In O_2 atmosphere, OMS-2 is stable up to a higher temperature of 600 °C and is progressively converted into bixbyite. TGA studies of M−OMS-2 materials in this research also indicate that, as a general trend, the metal cation doped M−OMS-2 materials have similar but slightly lower thermal stabilities than undoped OMS-2, especially when the dopant content is relatively high.

Comprehensive adsorption analysis confirmed that M−OMS-2 materials are porous materials containing micropores, which contribute 2% of total pore (up to 3000 Å) volume; mesopores, which contribute 54%; and macropores (500−3000 Å), which contribute 44%. The most probable pore size in the micropore range is about 5 Å and in the mesopore range is around 350 Å for M−OMS-2 materials. Although only about 2% of the total pore volume represents micropores in M−OMS-2 materials, about 20% of the total BET surface area (70−110 m^2/g) is contributed by micropores in the sample. Compared to undoped OMS-2, metal cation doped M−OMS-2 materials have slightly higher surface areas and pore volumes, especially when the dopant content is relatively high.

Basicity studies of synthetic M−OMS-2 materials with TPD of adsorbed CO_2 revealed that all M−OMS-2 materials prepared in this research have similar patterns of different basic sites with varied strengths and amounts after pretreatment. However, compared to MgO, the relative strengths and amounts of basic sites on the surface of M−OMS-2 materials are weaker and fewer, respectively. When compared to amphoteric γ-Al_2O_3, the amounts of very weak basic sites and moderate basic sites on the surface of M−OMS-2 materials are fewer, although they have more strong basic sites.

All prepared M−OMS-2 materials also have similar acidities, as revealed by TPD studies of NH_3. Compared to γ-Al_2O_3, the relative strengths and amounts of acid sites on the surface of M−OMS-2 materials are generally weaker and fewer.

Acknowledgment. We acknowledge the U.S. Department of Energy, Office of Basic Energy Science, Division of Chemical Sciences, and Texaco, Inc. for support of this research.

CM000868O

(34) Tanabe, K.; Misono, M.; Ono, Y.; Hattori, H. *New Solid Acids and Bases*; Elsevier: Amsterdam, 1989.

(35) Lahousse, C.; Bachelier, J.; Lavalley, J. C.; Lauron-Pernot, H.; Le Govic, A. M. *J. Mol. Catal.* **1994**, *87*, 329.

(36) Lauron-Pernot, H.; Luck, F.; Popa, J. M. *Appl. Catal.* **1991**, *78*, 213.